Solution Structure of Horse Heart Ferricytochrome c and Detection of Redox-Related Structural Changes by High-Resolution 1 H NMR † , ‡

ARTICLE *in* BIOCHEMISTRY · OCTOBER 1996

Impact Factor: 3.02 · DOI: 10.1021/bi961042w · Source: PubMed

3 AUTHORS, INCLUDING:

Phoebe X Qi
United States Department of Agriculture
45 PUBLICATIONS **1,317** CITATIONS
SEE PROFILE

Andrew Joshua Wand
University of Pennsylvania
193 PUBLICATIONS **8,719** CITATIONS
SEE PROFILE

Solution Structure of Horse Heart Ferricytochrome *c* and Detection of Redox-Related Structural Changes by High-Resolution ^{1}H NMR[†,‡]

Phoebe Xiurong Qi,[§] Robert A. Beckman,[||] and A. Joshua Wand*

Departments of Biological Sciences, Biophysical Sciences, and Chemistry and Center for Structural Biology, 816 Natural Sciences Complex, State University of New York at Buffalo, Buffalo, New York 14260-3000

Received May 1, 1996; Revised Manuscript Received July 9, 1996[⊗]

ABSTRACT: A model for the solution structure of horse heart ferricytochrome *c* has been determined by nuclear magnetic resonance spectroscopy combined with hybrid distance geometry−simulated annealing calculations. Forty-four highly refined structures were obtained using a total of 1671 distance constraints based on the observed magnitude of nuclear Overhauser effects and 58 torsion angle restraints based on the magnitude of determined *J*-coupling constants. The model incorporates six long-lived water molecules detected by pseudo-two-dimensional NOESY−TOCSY spectra. The all-residue root mean square deviation about the average structure is 0.33 ± 0.04 Å for the backbone N, Cα, and C′ atoms and 0.83 ± 0.05 Å for all heavy atoms. The overall topology of the model for solution structure is very similar to that seen in previously reported models for crystal structures of homologous *c*-type cytochromes though there are a number of significant differences in detailed aspects of the structure. Two of the three main helices display localized irregularities in helical hydrogen bonding resulting in bifurcation of main chain hydrogen bond acceptor carbonyls. The N- and C-terminal helices are tightly packed and display several interhelical interactions not seen in reported crystal models. To provide an independent measure of the accuracy of the model for the oxidized protein, the expected pseudocontact shifts induced by the spin $^1/_2$ iron were compared to the observed redox-dependent chemical shift changes. These comparisons confirm the general accuracy of the model for the oxidized protein and its observed differences with the structure of the reduced protein. The structures of the reduced and oxidized states of the protein provide a template to explain a range of physical and biological data spanning the redox properties, folding, molecular recognition, and stability of the cytochrome *c* molecule. For example, a redox-dependent reorganization of surface residues at the heme edge can be directly related to the redox behavior of the protein and thereby provides a previously undocumented linkage between structural change potentially associated with molecular recognition of redox partners and the fundamental parameters governing electron transfer.

Mitochondrial cytochrome *c* is a soluble 12.5 kDa protein that mediates single electron transfer between integral membrane protein complexes in the respiratory chain of eukaryotes. Because of its stability, solubility, and ease of preparation, cytochrome *c* has become one of the most thoroughly studied proteins. Several X-ray crystallographic studies have resulted in a number of high-resolution models of the crystal structures of *c*-type cytochromes. Although only subtle structural differences between redox states have been observed in these crystal models (Takano & Dickerson, 1981a,b; Berghuis & Brayer, 1992), a number of NMR-based structural studies suggest the presence of potentially significant structural differences [e.g., see Feng et al. (1990) and references therein]. Systems that include cytochrome *c* and various redox partners have also been used to investigate how the polypeptide chain assists in controlling electron transfer kinetics and thermodynamics (Onuchic et al., 1992; Farid et al., 1993). Experiments involving site-directed mutagenesis, semisynthesis, and chemical modification of cytochrome *c* have probed the role of several key amino acids involved in electron transfer [e.g., Wutke et al. (1992) and Willie et al. (1993)]. Interpretation of these and numerous other experiments, however, often relies on the availability of applicable high-resolution structural models. In an effort to help to clarify a variety of structural issues relating to the redox chemistry of this protein, we have undertaken the determination of the solution structures of horse cytochrome *c* in its two redox states. Here we describe the determination of a high-resolution model for the solution structure of horse heart ferricytochrome *c* using ^{1}H 2D and 3D NMR[1] spectroscopy and hybrid distance geometry−simulated an-

[†] This work was supported by NIH Research Grant GM-35940 and, in part, by NIH Grants CA-06927 and RR-05539, by an appropriation from the Commonwealth of Pennsylvania, and by a grant from the Fanny Rippel Foundation awarded to the Institute for Cancer Research. R.A.B. is the recipient of an NIH Physician Scientist Award (CA-01456). This paper is dedicated to Professor Lowell Hager on the occasion of his 70th birthday.

[‡] Coordinates of the refined average structures of reduced and oxidized cytochrome *c* along with the NMR-derived restraints have been deposited in the Brookhaven Protein Data Bank (PDB ID codes 2frc and 1ocd).

* To whom all correspondence should be addressed at the Department of Chemistry.

[§] Present address: Department of Chemistry, University of Illinois, 600 South Mathews Ave., Urbana, IL 61801.

[||] Present address: Chemistry Department, Parke Davis Pharmaceuticals, 2800 Plymouth Road, Ann Arbor, MI 48105.

[⊗] Abstract published in *Advance ACS Abstracts,* September 1, 1996.

[1] Abbreviations: COSY, *J*-correlated spectroscopy; DG, distance geometry; DQF, double-quantum filter; FID, free induction decay; NMR, nuclear magnetic resonance; NOE, nuclear Overhauser effect; pH*, pH meter reading uncorrected for the isotope effect; ppm, parts per million; rmsd, root mean square deviation; SA, simulated annealing; TOCSY, total correlation spectroscopy; EXAFS, extended X-ray absorption fine structure.

S0006-2960(96)01042-2 CCC: $12.00

nealing calculations. These detailed structural studies will hopefully provide the basis for a comprehensive reevaluation of hypotheses concerning the fundamental nature of the electron transfer processes in proteins. In particular, microscopic treatments of the role of redox-dependent structure change in the setting of fundamental parameters of the electron transfer process have led to a significant underestimation of the Marcus solvent reorganization energy (Churg et al., 1983). Using the structures reported here, we have undertaken a reevaluation of the solvent reorganization energy using a microscopic approach (I. Muegge, P. X. Qi, A. J. Wand, Z. T. Chu, and A. Warshel, in preparation). This analysis suggests the solution structures appear to provide an accurate template for these calculations with the obtained solvent reorganization energy and redox potential being quite close to that observed experimentally. Indeed, the analysis of the structures of the two redox states provides a direct mechanism for the energetic linkage of the redox and electron transfer properties of the protein and structural features which provide a mechanism for redox-dependent molecular recognition.

MATERIALS AND METHODS

Sample Preparation. Horse heart cytochrome *c* of the highest available grade was obtained from Sigma Chemical Co. and used without further purification. Sodium ascorbate and monobasic and dibasic potassium phosphate were reagent grade. Either 7 or 10 mM solutions of cytochrome *c* in 90% H_2O/10% D_2O containing 50 mM potassium phosphate (pH* = 5.75) were used for 2D NMR experiments, while a 15 mM solution was used to obtain a ^{1}H 3D NOESY−TOCSY spectrum.

NMR Spectroscopy. All NMR spectra were collected at 20 °C on Bruker AM-600 (600 MHz), AMX-500 (500 MHz), and AM-300 (300 MHz) NMR spectrometers. NMR spectra were processed and analyzed using the computer programs FTNMR and Felix (Biosym Technologies Inc.). NOESY (Macura & Ernst, 1980) spectra were recorded with mixing times of 30, 50, 70, 90, and 110 ms at 600 MHz with 64 scans per free induction decay (FID) using a 11 111 Hz spectral width. Each spectrum was derived from a data set composed of 700 FIDs, each consisting of 1024 complex data points. NOESY spectra with short mixing times (10 and 30 ms) were obtained at 300 MHz to measure NOEs involving extensively hyperfine-shifted resonances. High-resolution double-quantum-filtered COSY spectra (Rance et al., 1983) were also acquired in 90% H_2O/10% D_2O at 500 MHz and used to directly estimate $^3J_{H\alpha HN}$ coupling constants. Three-dimensional ^{1}H 3D NOESY−TOCSY spectra (Vuister et al., 1988) were acquired using a sample prepared in 90% D_2O/10% H_2O buffer with eight scans per free induction decay and were composed of 192 (t_1) × 192 (t_2) × 512 (t_3) complex points with spectral widths of 6410 Hz. A NOESY mixing time of 100 ms was used, and isotropic mixing was accomplished with a 30 ms MLEV-17 pulse train.

Distance Restraints. Previously reported assignments (Feng et al., 1989), supplemented with a small number of new assignments, for the ^{1}H NMR spectrum of horse heart ferrocytochrome *c* were used to identify cross-peaks in NOESY spectra. Initial rates of NOE buildups were estimated with local baseline correction of cross-peak volumes, calibrated using α helical main chain distance

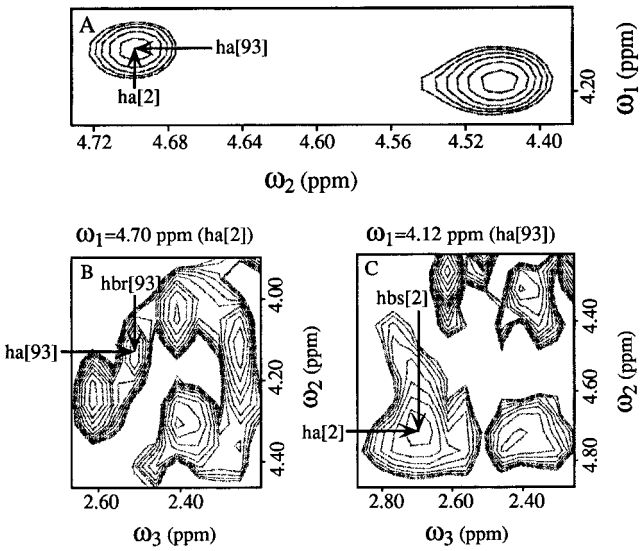

FIGURE 1: Sections of a 2D ^{1}H NOESY (A) and a 3D ^{1}H NOESY−TOCSY (B and C) spectrum of horse ferricytochrome *c* showing the NOE correlation between the Hα of Asp-93 and the Hα of Asp-2 in (A). Their *J*-correlations are shown in (B) and (C), respectively.

relationships (Wand & Nelson, 1991), and used to generate upper bounds for initial distance restraints. All upper bound restraints involving flipping aromatic rings were increased by 2.5 Å above that set by initial rates of NOE buildups. A lower bound distance restraint of 1.90 Å was applied. One round of structure calculations (see below) and iterative cross-peak assignment completed the initial set of NOE restraints. A structurally effective restraint set consisting of approximately 900 NOE-based distance restraints was thereby obtained from the 2D NOESY spectra. An additional set of 309 initial rate NOE-based distance restraints (Table 1) was obtained by evaluation of a family of 264 structures refined using the initial restraint set described above. Finally, an additional 462 restraints were derived from the analysis of a three-dimensional ^{1}H NOESY−TOCSY spectrum. The three-dimensional NOESY−TOCSY experiment does not provide simultaneous confirmation of the origin of both NOE-correlated frequencies. Thus, although confirmation of the origin of both frequencies could be checked by examining both NOESY−TOCSY pathways (i.e., spin A NOE to spin B TOCSY to spin C and spin B NOE to spin A TOCSY to spin D, as illustrated in Figure 1), this does not guarantee that a given cross-peak is entirely due to one spin pair. Therefore, initial structures were examined to provide an additional level of confidence on the assignment of a given NOE cross-peak to a given spin pair by rejecting all other possible spin pairs on gross structural grounds. To avoid issues relating to variable transfer efficiencies in the TOCSY component of the three-dimensional experiment, all restraints derived from analysis of the three-dimensional NOESY−TOCSY spectrum were simply encoded as corresponding to distance upper bounds of 5.0 Å [7.5 Å in the case of NOEs involving hydrogens of flipping aromatic rings and 6.0 Å in the case of methyl groups; see Dellwo & Wand (1993)] and a lower bound of 1.95 Å.

Torsion Angle Restraints. A high-resolution DQF-COSY spectrum was used to determine $^3J_{H\alpha HN}$ coupling constants. The $^3J_{H\alpha HN}$ coupling constants of 58 residues were estimated directly from the high-resolution DQF-COSY spectrum processed with strong resolution enhancement and corrected

Table 1: Origin of NOE-Based Distance Restraints Used in the Determination of the Solution Structure of Horse Heart Ferricytochrome *c*

origin of restraint	no. of 2D NOESY-based restraints	% of 2D NOESY-based restraints	no. of 3D NOESY−TOCSY-based restraints	% of 3D NOESY−TOCSY-based restraints	total NOE-based restraints	% of total NOE-based restraints
intraresidue (i,i)	453	37.5	93	20.1	546	32.7
interresidue (i,$i\pm1$)	263	21.8	67	14.5	330	19.7
interresidue (i,$i\pm2$)	34	2.8	20	4.3	54	3.2
interresidue (i,$i\pm j$), $3 \le j \ge 5$	167	13.8	203	17.1	246	14.7
interresidue (i,$i > 5$)	292	24.0	144	43.9	495	29.6
total	1209	100.0	462	100.0	1671	100.0

as described by Neuhaus et al. (1985). The empirical calibration constants of Pardi et al. (1984) were used to solve the Karplus equation (Karplus, 1959). The 58 determined ϕ torsion angle restraints were assumed to have a precision better than ±30°.

Initial Sampling of the Restraint Set. A metric matrix approach (Crippen, 1978; Havel, 1991) employing the program Dspace (Hare Research, Bothell, WA) was used to generate starting structures. The bounds matrix was created using amino acid templates as described previously (Beckman et al., 1993) and employed reduced van der Waals radii for atom pair interactions that could potentially be hydrogen bonding. The bounds matrix was smoothed by exhaustive application of the triangle inequality, randomly sampled and the structures embedded in E_3 space. The embedded structures were then refined with repetitive application of steepest descent least squares minimization of the sum of the squares of the violations of the structure with respect to covalent geometry and experimental restraints. At this stage of the refinement, errors in chirality were corrected by inversion. Minimization was then followed by several hundred cycles of simulated annealing using the sum of the squares of the violations as a pseudo-temperature variable (Nerdal et al., 1988).

Stereospecific Assignments. The floating chirality technique (Weber et al., 1988; Beckman et al., 1993) was used to obtain stereospecific assignments and employed the family of structures refined by simulated annealing in Dspace without hydrogen bond restraints. This procedure and the results with the oxidized protein are presented in detail elsewhere (Beckman et al., 1993). Iterative assignment of prochiral labels was not undertaken [see Beckman et al. (1993)].

Definition of Hydrogen Bond Restraints. A family of 264 structures, independently refined by simulated annealing in Dspace and each with not more than one violation greater than 0.5 Å, was used to assign definitive hydrogen bonding involving main chain atoms. The geometric criteria for hydrogen bonding employed required the amide nitrogen−carbonyl oxygen distance (d_{NO}) to be less than 2.5 Å and the angle formed by the amide nitrogen, amide hydrogen, and carbonyl oxygen to be greater than 120°. The statistical criterion used required that the geometric criteria be satisfied in *all* structures in order for a given hydrogen bond to be included as a restraint. This is a very stringent statistical requirement and was employed to avoid issues raised elsewhere (Beckman et al., 1993). A total of 14 hydrogen bonds were identified initially, each with the distance variations smaller than 0.5 Å and angle variations smaller than 40° within the family. These hydrogen bonds were incorporated as restraints by encoding them as simple distance bounds ($d_{OH} \le 1.95$ Å). Linearity was not required. All 264 structures were ultimately refined with Dspace using these hydrogen bond restraints to a sum of the squares of the violations less than 20 Å^2 and averaged less than two violations greater than 0.5 Å for each individually refined structure. A final set of 44 hydrogen bonds were identified and incorporated in the final stage of the refinement done by molecular dynamics as described in the next section.

Restrained Molecular Dynamics. The final refinement involving molecular dynamics calculations and restrained energy minimization was accomplished with the program X-PLOR (Brünger, 1992). Since the NOE restraint violations of the DG structures were relatively small at this stage, a standard refinement protocol was employed (Nilges et al., 1990). The empirical energy function of X-PLOR was applied and included terms to represent the covalent geometry, hard-sphere van der Waals interactions, and pseudoenergy terms to represent experimental distance and torsion angle restraints. No nonbonded, attractive potentials were employed. The force constant used to scale the van der Waals repulsion term was 4 kcal mol^{-1} Å^4. The NOE and torsion angle restraints were represented by a square well potential, and hydrogen bond restraints were represented by a soft square well potential, both of which were added to the remaining energy terms. The force constants were 50 kcal mol^{-1} Å^2, 1000 kcal mol^{-1} rad^{-2}, and 200 kcal mol^{-1} Å^{-2}, respectively. In the final stages of refinement, six water molecules were introduced into the model and restrained with simple distance bounds derived from observed NOEs (Qi et al., 1994b), using a force constant of 50 kcal mol^{-1} Å^{-2}.

RESULTS

Description of the Structural Restraints. The origin of the various NOE-based distance restraints derived from analysis of two-dimensional NOESY and three-dimensional NOESY−TOCSY spectra is summarized in Table 1. A total of 1671 unique NOE-based distance restraints were unequivocally identified and employed in the subsequent definition of the distance bounds matrix used to generate preliminary structures by embedding in E_3 space. Counting the heme prosthetic group,[2] this corresponds to nearly 16 NOE-based distance restraints per residue, which is comparable to the NOE-based restraint density used in previously reported determinations of high-resolution structures by these methods (Clore & Gronenborn, 1993). The majority (54%) of these restraints were derived from initial NOE buildup rates observed in NOESY spectra while the balance required the use of three-dimensional NOESY−TOCSY spectra and were therefore simply encoded as 5 Å upper bounds (see

[2] The heme nomenclature of the Brookhaven Protein Data Bank is used throughout (Bernstein et al., 1977). Refer to Berghuis and Brayer (1990) for a useful figure illustrating the labeling scheme.

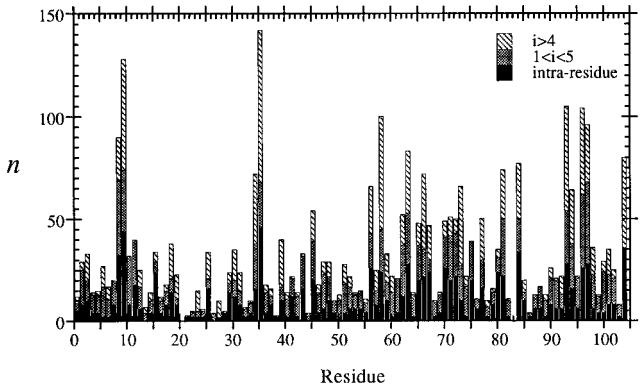

FIGURE 2: Summary histogram of the distribution and type of distance restraints used to define the model for the solution structure of horse ferricytochrome *c*. Shown are the number of NOE-based distances restraints (*n*) at each residue in the primary sequence derived from intraresidue (solid bars), short-range (less than five residues removed in the primary sequence) interresidue (shaded bars), and long-range (greater than four residues removed in the primary sequence) interresidue (hatched bars) distance restraints. The heme prosthetic group is shown as residue 105. In the histogram each interresidue restraint is represented twice, once at each residue involved. There are a total of 1671 unique NOE-based distance restraints.

Materials and Methods). A significant fraction of the NOE-based restraints involved residues more than five residues apart in the primary sequence. The distribution with respect to separation in the primary sequence of the residues related by NOE-based distance restraints is shown in Figure 2. ϕ torsion angle restraints were also obtained for 58 residues using direct measurements of a high digital resolution, extensively resolution-enhanced DQF-COSY spectrum to directly estimate the $^3J_{H\alpha HN}$ constants (Neuhaus et al., 1985).

Structural Statistics and Precision of the Structural Model. Following restrained simulated annealing of 264 independently generated structures, analysis of main chain hydrogen bonding was undertaken. Using the relatively stringent criteria outlined above, a total of 14 main chain hydrogen bonds were used in an iterative refinement cycle, and finally 44 main chain hydrogen bonds were identified and subsequently used as restraints in the final structural refinement (see Materials and Methods). After further restrained simulated annealing, a family of 44 structures was selected for further refinement and analysis. Selection was based upon lowest global penalty and fewest number of violations greater than 0.30 Å. The variance of this set of structures, {SA}, from the experimental restraints is summarized in Table 2. No member of the final set of refined structures had violations of experimental distance restraints greater than 0.50 Å, and each averaged only 0.18 violation of experimental distance constraints greater than 0.30 Å. No member of the final set of refined structures had violations of experimental restraints of ϕ torsion angles greater than 2°. Agreement with covalent geometry was generally excellent (Table 2). The refined average structure, $\langle SA \rangle_r$, showed similar levels of agreement with experimental distance and torsion angle restraints and assumed covalent geometry.

The family of final SA structures displays a level of variance about the average structure, $\langle SA \rangle$, or refined average structure, $\langle SA \rangle_r$, characteristic of typical high-resolution NMR-based structural models (Clore & Gronenborn, 1993). The all-residue average rmsd between the individual SA structures and the refined mean structure is 0.33 ± 0.04 Å for the backbone N, Cα, and C′ atoms and 0.83 ± 0.05 Å for all heavy atoms (Figures 3 and 4 and Table 2). One small region of the ferricytochrome molecule, residues 21−23, consistently showed rmsd from the simple mean structure over the family of SA structures greater than 0.50 Å on the main chain. Another small turn region, residues 37−38, also showed rmsd slightly greater than 0.50 Å on the main chain (see Figure 3). All other regions of the protein showed local

Table 2: Structural Statistics and Atomic Root Mean Square Deviations[a]

	{SA}	$\langle SA \rangle_{rw}$
violations of exptl restraints		
distance restraints (1671)		
no. ≥ 0.5 Å	0.00	0
no. ≥ 0.3 Å	0.18	0
ϕ torsion angle restraints (58)		
no. ≥ 5°	0.00	0
no. ≥ 2°	0.00	0
hydrogen bond distance restraints (44)		
no. ≥ 0.1 Å	0.00	0
rms deviations of all restraints		
NOEs (Å)	0.031 ± 0.001	0.033
ϕ torsional angles (deg)	0.116 ± 0.022	0.090
bonds (Å) (1772)	0.004 ± 0.000	0.005
angles (deg) (3240)	0.881 ± 0.125	1.030
impropers (deg) (706)	0.489 ± 0.020	0.480

comparison	backbone atoms	all heavy atoms	all atoms
atomic rms deviations (Å)			
{SA} vs $\langle SA \rangle$	0.329 ± 0.042	0.832 ± 0.050	1.124 ± 0.054
{SA} vs $\langle SA \rangle_r$	0.375 ± 0.048	0.956 ± 0.064	1.343 ± 0.068
{SA} vs $\langle SA \rangle_{rw}$	0.430 ± 0.048	1.014 ± 0.055	1.399 ± 0.060
$\langle SA \rangle_r$ vs $\langle SA \rangle$	0.182	0.473	0.736
$\langle SA \rangle_r$ vs $\langle SA \rangle_{rw}$	0.258	0.395	0.485
$\langle SA \rangle$ vs $\langle SA \rangle_{rw}$	0.278	0.581	0.833

[a] The notation of the structures is as follows: {SA} is the set of 44 final simulated annealing structures; $\langle SA \rangle$ is the simple mean structure obtained by averaging the coordinates of the 44 individual SA structures superimposed to each other; $\langle SA \rangle_r$ is the structure obtained by restrained minimization of $\langle SA \rangle$; $\langle SA \rangle_{rw}$ is the structure obtained by steepest descent restrained minimization of $\langle SA \rangle_r$ with six structural waters introduced using a total of 38 distance restraints. In all comparisons, noted atom types of all residues were included.

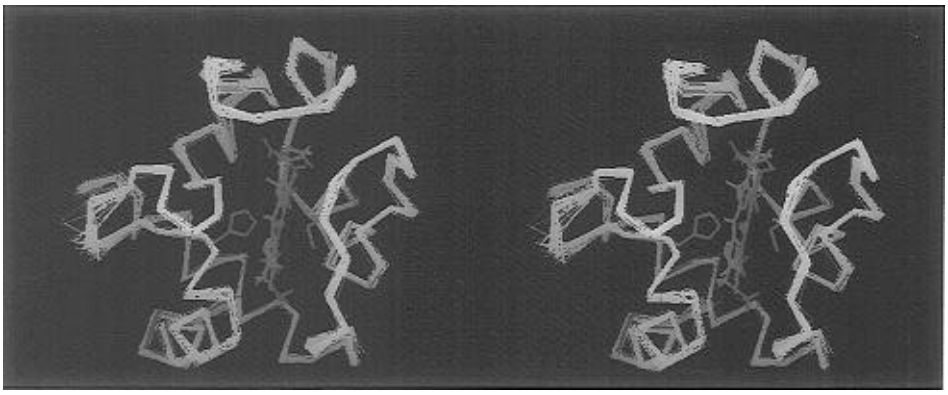

FIGURE 3: Variance of the family of final refined SA structures of horse heart ferricytochrome *c*. Shown are stereo pairs of the α-carbon tracings of the 44 SA structures in yellow superimposed on the $\langle SA \rangle_{rw}$ structure shown in red. The heme prosthetic group and the two axial ligands, His-18 and Met-80, of the average structure are shown in red.

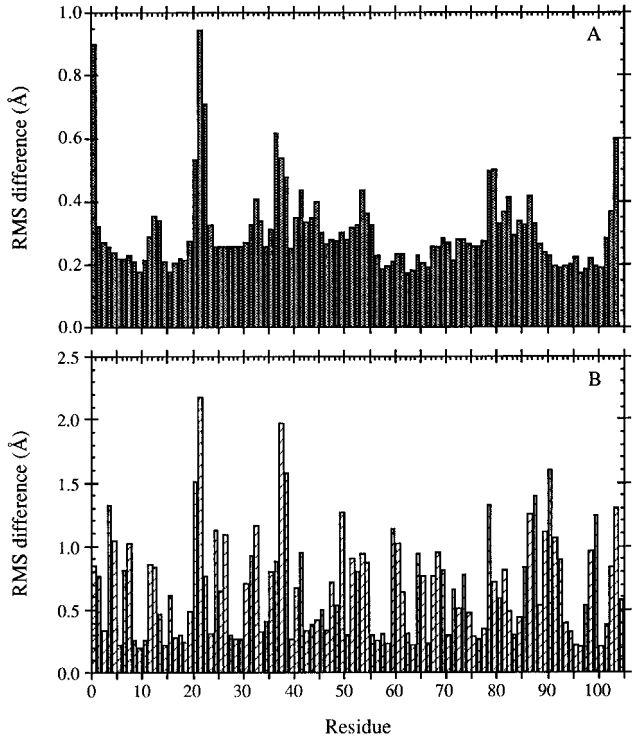

FIGURE 4: Analysis of the variance of the family of final refined structures from the average structure, ⟨SA⟩, of horse ferricytochrome *c*. Shown are the average rmsd following all-residue superposition of the backbone N, Cα, and C′ atoms (panel A) and all non-hydrogen atoms (panel B) of each SA structure to the average structure.

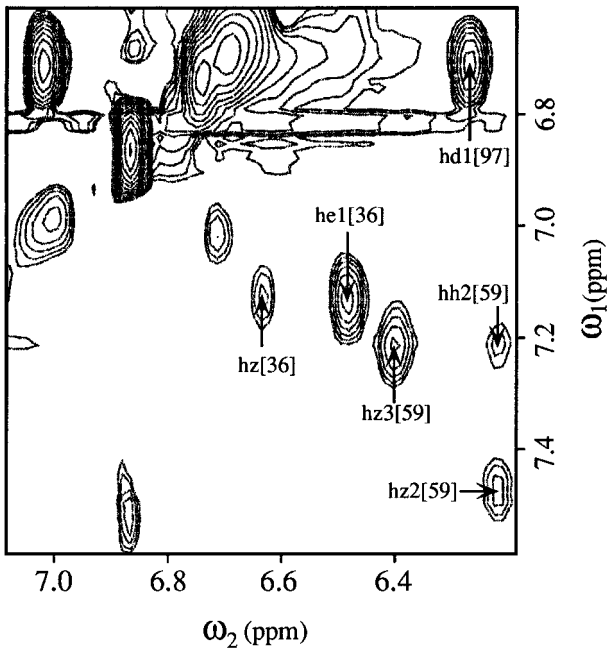

FIGURE 5: Section of a ^{1}H NOESY−TOCSY NMR spectrum where the water has been selectively excited and the resulting NOEs have been resolved in two dimensions by total correlation spectroscopy. Long-lived (>300 ps) structural water molecules are detected by this approach. A number of NOE cross-peaks that have been used as distance restraints in the final refinement of $\langle SA \rangle_{rw}$ are labeled.

backbone rmsd between the mean and individual SA structures significantly less than 0.50 Å. The high degree of correspondence of the backbone among the individual SA structures is illustrated by Figures 3 and 4. Similarly, the majority of side chains are also well defined. A number of side chains, however, do have atomic rmsd from the ⟨SA⟩ coordinate positions larger than 1 Å. All of these side chains have extensive solvent accessibility including many of the 19 lysine residues. As expected, buried side chains have atomic rms distributions about the mean coordinate positions significantly less than 1.0 Å (Figure 4). Three small clusters of three to four ill-defined side chains, centered on residues 22, 37, and 88 in the primary sequence, are all highly accessible to solvent.

Structural Water. The $\langle SA \rangle_r$ model for the solution structure of horse ferricytochrome *c* allows for the placement of structural waters detected by NMR (Qi et al., 1994b). An example of NOEs between a structural water and protein residues is shown in Figure 5. The six waters that were determined to be long lived (i.e., lifetimes greater than 300 ps) were introduced into the $\langle SA \rangle_r$ by use of simple distance restraints to the water molecule; no attractive potentials were employed. A total of 38 restraints to the six water molecules were incorporated. The model was refined using restrained minimization; no simulated annealing was required. The resulting structure ($\langle SA \rangle_{rw}$) differed very little from the $\langle SA \rangle_r$ structure and showed a similar variance from the {SA} family of structures (Table 2). The water molecule designated Wat-1 is located at the center of an interaction involving the side chains of Tyr-74, Ile-75, and Thr-78; the amide hydrogens of Thr-48 and Lys-53 are also involved. A second water molecule, designated Wat-2, is located in the crevice formed by the amide and α-hydrogens of Thr-19 as well as the side chains of Asn-31. A third water molecule, Wat-3, is located in the rough turn at residues 42−46. The fourth water molecule was located between the α-

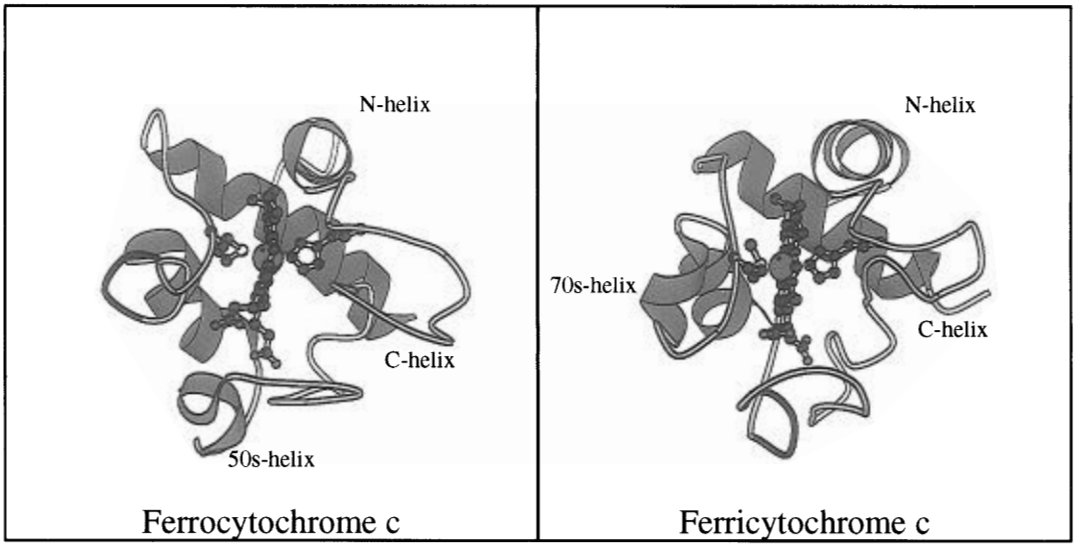

FIGURE 6: Schematic representations of the refined average models, $\langle SA \rangle_{rw}$, for the structures of oxidized (right) and reduced (left) horse heart cytochrome *c*. Drawn with the program Molscript (Kraulis, 1991).

and β-hydrogens of Ala-83, the side chains of Ile-81, and the β-hydrogens of Asn-70. A fifth water is located in the groove of a series of side chains of Ile-57, Trp-59, and Tyr-67. Finally, a sixth water is found in the turn region containing Leu-35, Phe-36, and the aromatic ring hydrogens of Tyr-97. Four out of the six water molecules have been seen in roughly analogous positions in a variety of crystal structures [e.g., Bushnell et al. (1990) and Takano and Dickerson (1981a,b)], while all of them have been identified in similar positions in the model of solution structure of ferrocytchrome *c* (Qi et al., 1994a; see footnote 3 and Supporting Information). This structure, referred to below as $\langle SA \rangle_{rw}$, is being deposited in the Brookhaven Protein Data Bank (Berstein et al., 1977) under identification code (code to be provided).

Analysis of Secondary Structure Elements. Elements of secondary structure were identified using both Ramachandran ϕ, ψ plots and the analysis of main chain hydrogen bonding (Supporting Information). A schematic representation of the $\langle SA \rangle_{rw}$ model for the solution structure of ferricytochrome *c* is shown in Figure 6. Included for comparison is the further refined structure of the reduced protein (Qi et al., 1994a).[3] The geometrical hydrogen-bonding criteria were based on the analysis of Rose and co-workers (Stikle et al., 1992) and are, for the hydrogen bond system D′D−D−H A−AA′, as follows: the distance between the acceptor and the hydrogen (d_{HA}) must be less than 2.5 Å, the distance between the electronegative heavy atoms in a hydrogen-bonded pair (d_{AD}) must be less than 3.4 Å, the D−H−A angle must be greater than 90°, and the angle between the normals of the planes (D−DD−DD′) and (A−D−DD′) must be less than 60°. These criteria are somewhat less stringent than those used to define hydrogen bond restraints (see Materials and Methods). Each SA structure was investigated, and a running tally of the hydrogen bonds found is summarized in Supporting Information. A similar analysis of the model of the solution structure of reduced horse cytochrome *c* and the hydrogen bonding for the crystal structures of reduced and oxidized horse cytochrome c (Bushnell et al., 1990) are also provided in Supporting Information.

In general, the secondary structure content and distribution and corresponding hydrogen-bonding patterns seen across the family of SA structures are highly homologous to those seen in previously reported models for the crystal structures of eukaryotic *c*-type cytochromes and that of the solution structure of horse ferrocytochrome *c*. It is clear, however, that there are several significant differences in the details of the hydrogen-bonding network, particularly along the backbone. The three major helices characteristic of the *c*-type cytochrome fold are present in the model for the solution structure of horse ferricytochrome *c*. The helix spanning residues 60−70 is terminated by a β-turn (type III, 3_{10}) from Tyr-67 to Asn-70 at residue Glu-68, in consistent with the recently deposited crystal structure for reduced horse heart cytochrome *c* as well as the solution structure of ferrocytochrome *c* (Qi et al., 1994a). The transition to a 3_{10}-helix involving residues 60−63 that is observed in the solution structure of ferrocytochrome *c* is not present in the oxidized protein. The α-helix spans residues 60−70 and has an N-terminal cap involving the hydroxyl of Thr-63 and the amide hydrogen of Lys-60 as is also seen in the model for the solution structure for ferrocytochrome *c* (Qi et al., 1994a).

The N-terminal α-helix begins α-helical $i \rightarrow i + 4$ hydrogen bonding with Val-3, continues until Cys-14, and ends with a type III β-turn between residues Cys-14 through Cys-17. There is a 3_{10} hydrogen bond between the amide hydrogen of Lys-5 and the carbonyl of Asp-2. The 3_{10} hydrogen bond between the amide hydrogen of Cys-14 and the carbonyl of Cys-17 observed in the crystal structure is not apparent in the solution structure. Only a small number of the family of 44 {SA}s in ferrocytochrome *c* showed close hydrogen-bonding geometry (see Supporting Information). Nevertheless, pairwise comparison among various structural models showed that it is a well-conserved region with rmsd

[3] The previously reported model for the solution structure of ferrocytochrome *c* has been further refined with 52 hydrogen bonds involving main chain atoms and an additional 33 distance restraints added to the original restraint set (Qi et al., 1994a). The statistics summarizing the final model are given in the Supporting Information. Overall, the final structure varies very little from that reported previously (Qi et al., 1994a) with the exception of two loop regions (22−24 and 89−91). The new model has been deposited in the Protein Data Bank under identification code 2frc.

Table 3: Heme Iron Coordination Geometry

	{SA}		⟨SA⟩		$\langle SA \rangle_{rw}$		
	ferri	ferro	ferri	ferro	ferri	ferro	crystal,[a] ferro
His-18 NE2 (Å)	2.00 ± 0.05	1.89 ± 0.02	1.98	1.88	2.06	1.92	2.04
Met-80 SD (Å)	2.36 ± 0.06	2.24 ± 0.04	2.32	2.23	2.44	2.23	2.32
heme NA (Å)	1.95 ± 0.005	1.95 ± 0.002	1.95	1.94	1.96	1.95	2.01
heme NB (Å)	1.96 ± 0.004	1.95 ± 0.002	1.96	1.94	1.96	1.95	1.95
heme NC (Å)	1.95 ± 0.004	1.94 ± 0.003	1.95	1.94	1.95	1.94	2.04
heme ND (Å)	1.95 ± 0.004	1.95 ± 0.001	1.94	1.94	1.95	1.95	1.98
His-18 NE2−Fe−Met-80 SD (deg)	160.6 ± 4.8	168.0 ± 3.5	160.8	169.5	152.0	161.4	171.9

[a] 1hrc (Brookhaven Protein Data Bank); Luo et al., 1994.

for the backbone atoms less than 0.5 Å between each pair. The termination of the N-terminal helix by a type I β-turn is well characterized by the hydrogen bond formed between the amide hydrogen of Glu-104 and the carbonyl of Ala-101 in all 44 {SA} structures. In contrast, this β-turn is only seen in some of the {SA} structures in the solution structures of ferrocytochrome *c* and is not evident in the model of the crystal structure of horse ferricytochrome *c* (Bushnell et al., 1990).

A number of regions (residues 21−24, 32−35, 35−38, 75−78), all of which are solvent accessible, show subtle differences between the solution structures and the crystal structure. Specific β-turns initially classified in a number of cytochrome *c* crystal structures [e.g., Takano and Dickerson (1981a,b) and Bushnell et al. (1990)] do not neatly fall into such classifications in either of the solution structures, and the 3_{10} hydrogen-bonding pattern shows irregularity (Supporting Information). With the exception of the regions including residues 21−24 and residues 37−38, these regions of the main chain are well defined, and therefore the inability to formally classify these turn regions is not due to an underlying lack of definition of the structural model.

Residues 49−54 are helical in the models for the crystal structures of horse ferrocytochrome *c* and ferricytochrome *c* (Bushnell et al., 1990). Similarly, the model for the solution structure of ferrocytochrome *c* displays a helical segment spanning these same residues. In contrast, the model for the solution structure of ferricytochrome *c* has two non-α-helical turns in place of the helix. The analysis across the entire family (Supporting Information) resulted in the classification of these turns. The first β-turn (type III) has a 3_{10} hydrogen bond between the carbonyl of Ala-51 and the amide hydrogen of Asn-54, and a second turn is defined by a 3_{10} hydrogen bond between Asn-52 and Lys-55. Residues Asn-70 through Ile-75 form a short 3_{10}-helix in the solution structure but are seen to form an α-helix in the reduced and oxidized crystal structures. This region is a series of turns in the solution structure of the reduced protein (Qi et al., 1994a).

Tertiary Structural Features. There are a number of hydrogen bonds associated with the tertiary structure. The N- and C-terminal helices are linked by several hydrogen bonds and a salt link. The amide hydrogens of Asp-2 and Val-3 and the side chain carbonyl of Asp-93 are hydrogen bonded in the oxidized protein as they are in reduced cytochrome *c*. The side chains of Lys-5 and Asp-93 are also consistently close, indicating the potential for formation of a salt link.

As with the model for the solution structure of the reduced protein (Qi et al., 1994a) a clear disappointment with the current structural model for the oxidized state is the apparent lack of definition of hydrogen bond donors for the propionate groups of the heme. These interactions have been implicated as being important with respect to both dynamics and structure. Unfortunately, the carboxyl groups of the propionates are only indirectly restrained; i.e., there are no direct restraints on the rotamer adopted. Accordingly, the carboxyl groups of both propionates are relatively disordered and make assignment of interactions to them difficult. The side chain NH of Trp-59, which has been found to be hydrogen bonded to the heme A ring propionate, is consistently close across the family of SA structures but shows inconsistent hydrogen-bonding geometry.

The geometry of the heme and the axial ligands in the model for the solution structure of horse ferricytochrome *c* and models of the crystal structures of eukaryotic cytochromes *c* are generally equivalent (Table 3). The heme remains nonplanar with a distorted saddle-shaped geometry. The atomic distance between NE2 of His-18 and the heme Fe and the distance between the sulfur of Met-80 are nearly the same in each structure.

The interior side chains of the amino acids packing against the heme prosthetic group are in general very well defined. The aromatic ring of Phe-82, which is believed to play an important role in the electron transfer process, is well defined across the complete family of SA structures. The distances between CZ and CG atoms of Phe-82 and the heme iron are 8.29 ± 0.31 and 7.08 ± 0.18 Å, respectively, for a family of 44 SA structures, as opposed to 8.06 and 6.32 Å in the crystal model for ferricytochrome *c* (Pelletier & Kraut, 1992) and 7.93 and 6.52 Å for the crystal model for ferrocytchrome *c* (Bushnell et al., 1990). In comparison, the ferrocytochrome *c* model displays distances of 5.82 ± 0.22 and 6.26 ± 0.18 Å, respectively.

As illustrated by the space-filling model presented in Figure 7, the heme group is nearly completely buried. Only about 15% of the potential accessible surface area of the heme is accessible to solvent (Table 4). This value is about twice as much as that in the reduced solution structure (Qi et al., 1994a) or the crystal structure (Bushnell et al., 1990). The significant differences are in the distribution of accessible surface area along the heme edge (Figure 7). For example, CBC has significant solvent accessibility in the solution structure of ferricytochrome *c* but is essentially buried in the crystal structure. Furthermore, CMC is significantly more solvent accessible in the oxidized state and less in the solution and crystal structures of the reduced protein. The differences in the surface accessibility of the front edge of the heme are primarily due to the differences in surface alignment of the residues involved in heme packing. Variation of the surface accessibility of the heme with a change

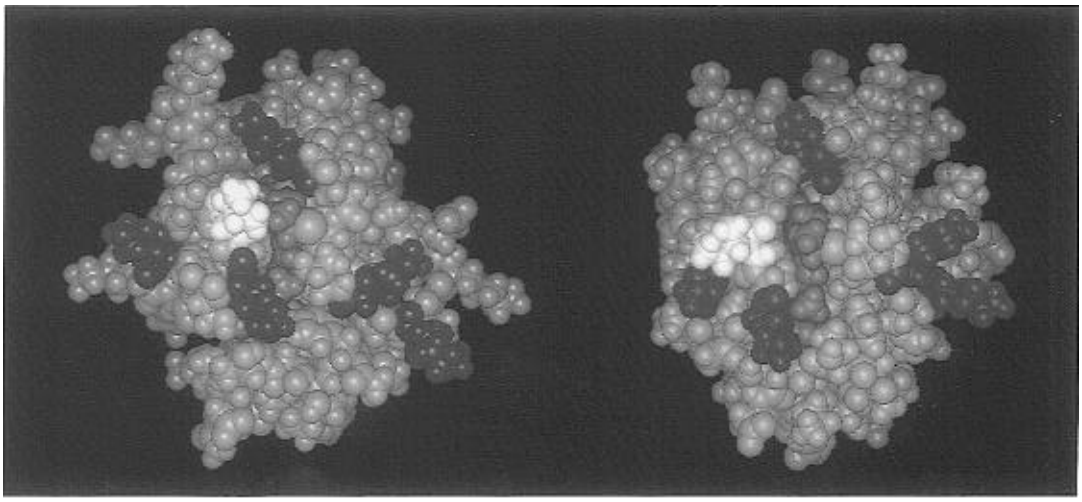

FIGURE 7: Space-filling representation of the $\langle SA \rangle_{rw}$ models for the solution structures of horse heart ferricytochrome *c* (right) and ferrocytochrome *c* (left) showing the exposed heme edge and annulus of lysine side chains thought to be important in docking of the protein with electron transfer partners. The heme edge is colored red, the side chains of Lys-13, Lys-25, Lys-27, Lys-72, and Lys-79 are colored blue, and the side chain of Ile-81 is shown in white. Drawn with the program Insight II (Biosym Technologies).

Table 4: Comparison of Heme Solvent Accessibility in Reduced and Oxidized Horse Heart Cytochrome *c*

	solution structure $\langle SA \rangle_{rw}$		
solvent-accessible area (Å^2)	ferri	ferro	crystal structure,[a] ferro
CHD	0.0	0.0	0.0
CAC	1.6	0.67	0.02
CBB	0.0	4.0	0.0
CBC	25.8	14.8	17.1
CMC	6.3	1.4	3.6
CMD	4.0	0.88	0.28
O1D	0.0	0.0	0.0
total heme exposure (Å^2)	62.7	33.2	30.8
calcd total heme exposure area (Å^2)	428.0	441.0	446.4
heme surface area exposed (%)	14.6	7.53	6.90

[a] 1hrc (Brookhaven Protein Data Bank); Luo et al., 1994.

in redox state provides a clear mechanism to modulate the redox potential of the protein (Kassner, 1972).

Assessment of Accuracy—Electron Spin g-Tensor Calculations. Though ferrocytochrome *c* is diamagnetic, ferricytochrome *c* is paramagnetic, having an electronic spin of $^1/_2$. The paramagnetic center contributes an additional term to the observed chemical shift via hyperfine interactions leading to so-called contact and pseudocontact shifts. For any given hydrogen, the observed redox-dependent change in chemical shift, $\Delta\delta_{obs}$, can be described as

$$\Delta\delta_{obs} = \delta_{ox} - \delta_{red} = \Delta_C + \Delta_{PC} + \Delta_D \qquad (1)$$

where δ_{ox} and δ_{red} are the observed chemical shifts in the oxidized and reduced proteins, respectively, and Δ_C and Δ_{PC} correspond to the chemical shift changes caused by Fermi contact and pseudocontact interactions between the hydrogen nucleus and the unpaired electron spin, respectively. Chemical shift changes brought about by a change in the diamagnetic term, Δ_D, arise from a change in the structure of the protein upon a change in redox state. The pseudocontact contribution is defined by the electronic *g*-tensor (Kurland & McGarvey, 1970; Horrocks & Greenberg, 1971)

$$\Delta_{PC} = [\beta^2 S(S-1)/9kTr^3][g_{ax}(3\cos^2\theta - 1) + 1.5g_{eq}(\sin^2\theta \cos 2\phi)] \qquad (2)$$

where β is the Bohr magneton, S is the electron spin quantum number, T is the absolute temperature, g_{ax} and g_{eq} are the axial and equatorial anisotropies of the *g*-tensor, and r, θ, and ϕ are the polar coordinates of the hydrogen in the *g*-tensor reference frame. In the past, positions of structure change upon a change in redox state were examined by comparing the redox-dependent chemical shift changes to that predicted by the crystal structure of the oxidized protein and eq 2 (Feng et al., 1990; Williams et al., 1985). In the context of the current effort, these relationships afford an opportunity to independently assess the accuracy of the structural models of reduced and oxidized cytochrome *c* by comparing the observed and predicted redox-dependent changes in chemical shift. Thus, electron spin *g*-tensor calculations were carried out in an attempt to further investigate the structural differences between the two redox states of the protein (Figure 8). Following the criteria of Feng et al. (1990), a set of 57 α-hydrogen resonances were selected to be used as a basis for determining the fundamentals parameters describing the g-tensor. The α-protons of residues 2−12, 16, 22, 25, 27, 32, 33, 35, 36, 38, 39, 43, 47, 50, 57−66, 69, 70, 72, 73, 76, 82, 85, 87−98, and 100−104 were selected as the reference set. The explicit search for the *g*-tensor parameters giving the lowest sum of the squares of the deviations between observed and predicted redox-dependent chemical shift changes using these reference hydrogens and the $\langle SA \rangle_{rw}$ structure led to best fit values for

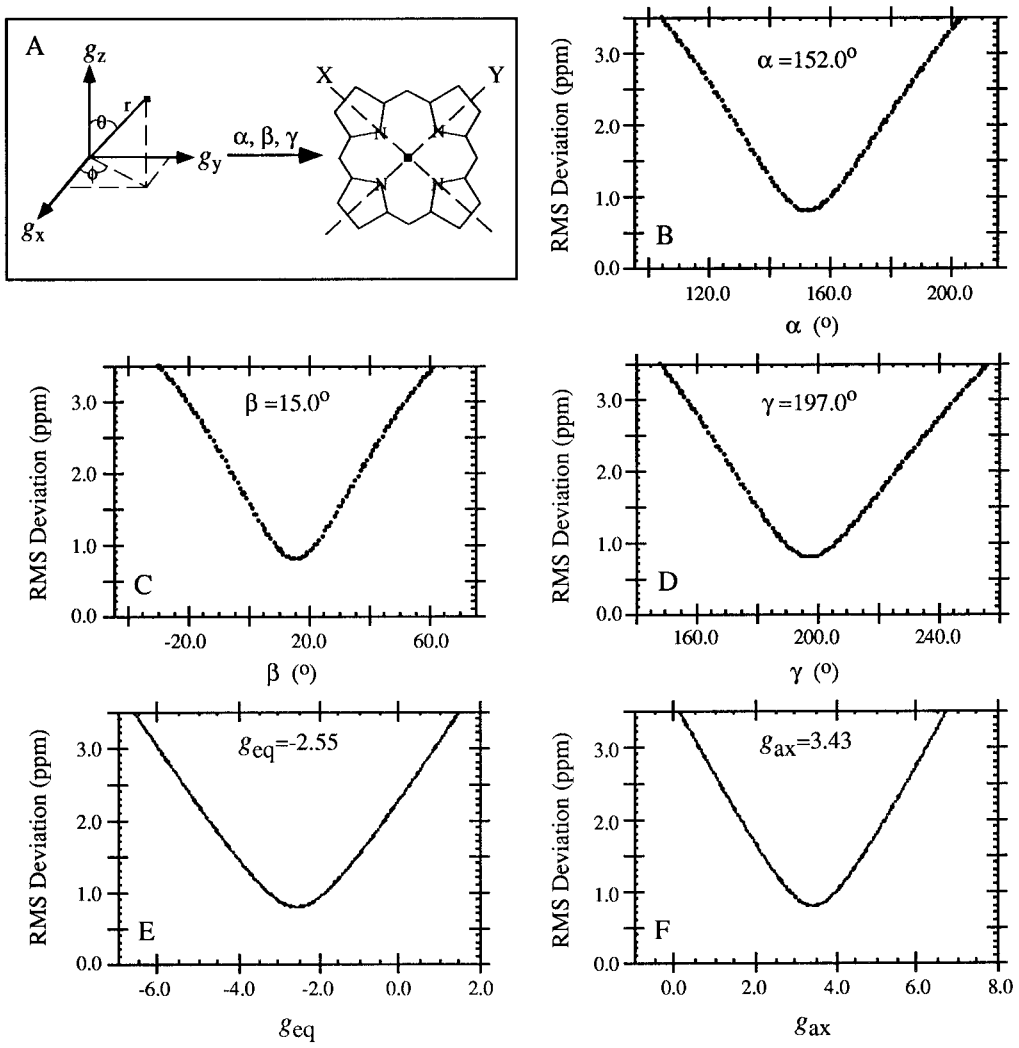

FIGURE 8: Determination of the electronic *g*-tensor parameters. Panel A shows the coordinate system used to align the *g*-tensor in the molecular frame. The successive rotation angles (α, β, γ) used to align the *g*-tensor were determined using a reference set of Hα resonances and a simple least squares criterion. Panels B, C, and D show the well-defined minima of the sum of the rmsd of the observed redox-dependent chemical shift changes of the reference set as a function of α, β, and γ, respectively. Panels E and F show similar plots for the optimization of the *g*-tensor anisotropy values, g_{eq} and g_{ax}, respectively.

g_{ax}, g_{eq}, α, β and γ of -2.55, 3.43 and 152°, 15°, and 197°, respectively (Figure 8). The determined rotation angles agree reasonably well to those determined by Feng et al. (1990) using a crystal model. The anisotropy terms, however, do not agree as well (5.15 and -1.65 versus 3.43 and -2.55). Nevertheless, the average rms deviations of the reference set for the solution model are on the same order as those used in the previous analysis based on the crystal model (0.006 versus 0.004 ppm) (Feng et al., 1990).

Having determined the basic parameters of the *g*-tensor, one can use the large deviations between predicted pseudocontact shifts and observed redox-dependent shifts to point to regions of redox-dependent structure change that lead to a significant change in the diamagnetic contribution to the chemical shift of a given hydrogen resonance. A general estimate of the degree of accuracy of the model for the solution structure of horse ferricytochrome *c* can be derived from the degree of agreement between the predicted and observed redox-dependent chemical shift changes of both the reference set and those hydrogens which did not pass the selection criteria. As illustrated by Figure 9, the main chain α-hydrogens which comprise the reference set and span essentially the whole molecule show small deviations from the chemical shift changes predicted, generally well under an estimated 0.3 Å deviation. Additionally, significant deviations of non-reference hydrogens are clustered in regions of significant structural differences between reduced and oxidized cytochrome *c* (Figure 10).

Recently, it has been pointed out that the availability of an independent measure of structure, pseudocontact shifts induced by the electronic *g*-tensor, provides a potential means of further refinement of a structural model (Gochin & Roder, 1995). Here, we have encoded the structural restraints by finding those spherical coordinates which satisfy eq 2 for a given observed $\Delta\delta$, assuming that the entire effect is due to the pseudocontact term. Equation 2 is degenerate so the $\langle SA \rangle_{rw}$ model was used to select the appropriate solution. The obtained solution was encoded as a set of distance restraints to the heme iron and pyrole nitrogens with a nominal bound width of 0.5 Å. This approach is quite different than that used by Gochin and Roder (1995), where the Δ_{PC} term was calculated "on the fly" during simple least squares minimization in the absence of other experimental constraints. As the Δ_{PC} term is invariant to the details of the molecular model beyond the basic geometric relationships defined by eq 2, the approach of Gochin and Roder (1995)

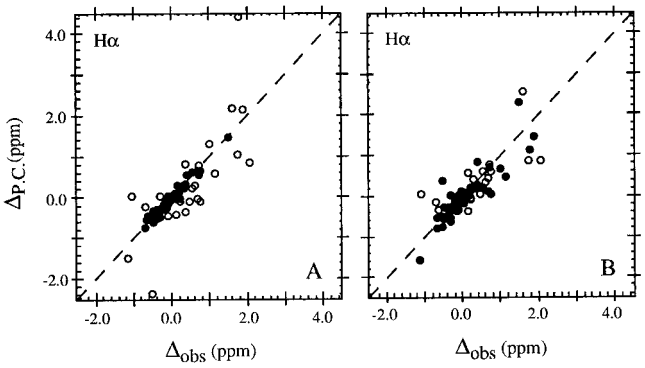

FIGURE 9: Comparison of measured redox-dependent chemical shifts and calculated pseudocontact shifts for Hα resonances of horse ferricytochrome *c*. The calculated pseudocontact shifts using the determined structure ($\langle SA \rangle_{rw}$) are plotted against the observed redox-dependent chemical shift change (panel A). Solid symbols correspond to those α-hydrogens used in the reference set to determine the *g*-tensor parameters. Panel B shows the predicted chemical shift (Δ_{PC}) obtained with the $\langle SA \rangle_{rw}$ model using a set of restraints based on the correspondence of the predicted pseudocontact shift to the observed redox-dependent chemical shift change (Δ_{obs}). Solid symbols correspond to those α-hydrogens incorporated into the restraint set.

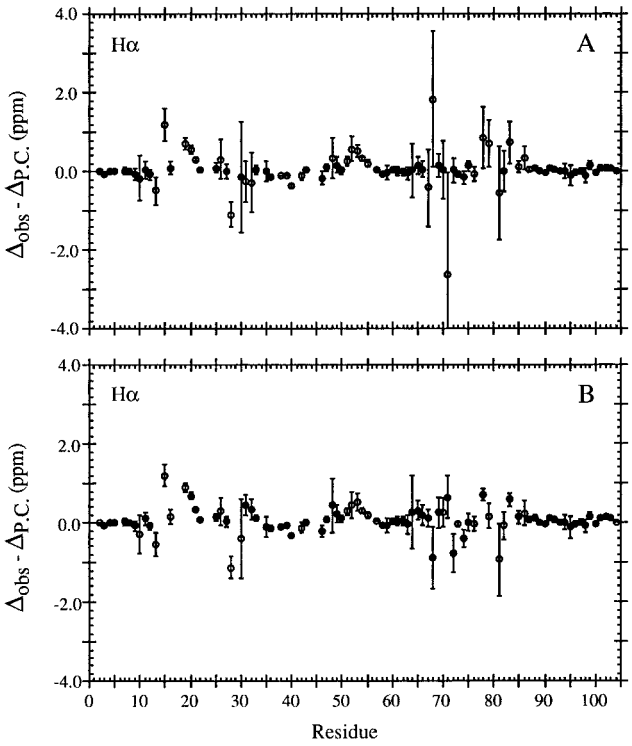

FIGURE 10: Location of redox-dependent structure change as indicated by deviations between the predicted and observed redox-dependent chemical shift change for α-hydrogen resonances. Panel A shows the degree of correspondence of the redox-dependent chemical shift changes of the set of selected hydrogen resonances with the predicted pseudocontact shift term calculated using the $\langle SA \rangle_{rw}$ model. Solid symbols represent those α-hydrogens used in the reference set to determine the parameters of the electronic *g*-tensor. The vertical error bars represent the predicted maximal change in the pseudocontact shift upon a change in position of 0.3 Å [see Feng et al. (1990)]. Significant deviations are located in the ω-loop (residues 20−30), near the axial ligands to the heme (residues 18 and 80) and in the small helical region including residues 50−55. These results are consistent with the independently determined solution structures (see text). Panel B shows the same relationship after further refinement of the $\langle SA \rangle_{rw}$ model with the geometry required by the pseudocontact shift term in the experimental restraint set. Solid symbols correspond to those α-hydrogens used in the pseudocontact shift-based restraint set for refinement of the $\langle SA \rangle_{rw}$ model.

is unnecessary except when one is able to couple explicit calculations of the diamagnetic contribution directly into the refinement.

On the basis of the pseudocontact shift analysis, a set of 435 additional distance bounds were used to restrain the geometry of 87 atoms relative to the heme by restraining the distance between a given atom and the iron and four pyrole nitrogens of the heme. The 12 glycines were excluded because of potential ambiguity in the assignment of prochiral labels. Cysteines 14 and 17 and the two axial ligand residues, His-18 and Met-80, were excluded because of possible contamination by Fermi contact contributions. Each distance bound used was spread by 0.25 Å across the distance indicated by the observed redox-dependent chemical shift change using the *g*-tensor parameters defined above. This set of distance restraints was equally weighted with NOE-based distance restraints and employed the same force constant. Restrained steepest decent energy minimization resulted in a decrease in the average rms deviation of the predicted pseudocontact chemical shift from the observed redox-dependent chemical shifts from 0.459 to 0.346 ppm for the *entire* set of 87 α-hydrogens. The all-residue all-heavy atom superposition of the starting and ending models indicates only a small difference between the two (∼1.3 Å all-atom−all-residue ⟨rmsd⟩) with most differences concentrated in regions of redox-sensitive chemical shift change, as expected.

DISCUSSION

The overall topology of the $\langle SA \rangle_{rw}$ model for the horse ferricytochrome *c* solution structure determined here and that seen throughout the *c*-type cytochrome family is the same. Variation of ionic strength between the solution and crystal structures of *c*-type cytochromes appears to leave the details of the heme ligation unaffected. However, some potentially significant differences do emerge at the secondary and tertiary levels of structural organization. In particular, the degree of contact between the N- and C-terminal helices is more intimate than that seen, for example, in the crystal structure model of horse heart ferricytochrome *c* (Bushnell et al., 1990; Pelletier & Kraut, 1992) and is similar to the solution structure model of horse heart ferrocytochrome *c* (Qi et al., 1994a). In fact, the indication of a salt link and tertiary hydrogen bonding between these two secondary structural elements is consistent with the apparent cooperative folding (Roder et al., 1988) and inherent stability of these two elements (Wu et al., 1993).

An interesting feature of the oxidized solution structure of cytochrome *c* is the absence of a well-formed helix spanning residues 50−55, present in both oxidized crystal structures and the reduced solution structure and replaced by a series of turns in the oxidized solution structure. The 60's helix in the reduced solution structure contains a 3_{10} component which is also absent in the crystal structure.

Comparison between Solution and Crystal Structures. The basic *c*-type cytochrome fold is seen in the solution structure of ferrocytochrome *c* (Qi et al., 1994a) and in both the solution and crystal structures of ferricytochrome *c* (Bushnell et al., 1990; Pelletier & Kraut, 1992). The three major helices are present in all the structures, and the details of

heme ligation are very similar. Detailed aspects of the secondary structure, however, differ between the two classes of structural models. These differences mainly concern surface loops and turns that are solvent accessible. Specifically, the regions of most variability span residues 21−24 and 35−38. When a pairwise comparison using only backbone atoms encompasses any of the three major helices, the rms deviations are significantly below 1.0 Å among all the structures. Upon close examination, one notes that according to rms deviation, the reduced solution (Qi et al., 1994a) and the crystal (Bushnell et al., 1990) structures resemble each other to a greater extent than the oxidized and reduced solution structures. This can be most easily seen by examining the rms deviation at the Cα level individual secondary structural fragments between residues 1−104 for the two final oxidized and reduced solution and reduced crystal structure. The average rms differences for the entire molecule are approximately 3.0 Å between the two final solution structures and the family of structures in the opposite redox state. In contrast, a rms deviation of about 2.0 Å is seen for the pair of oxidized ($\langle SA \rangle_{rw}$) and reduced ($\langle SA \rangle_{rw}$) solution structures against the reduced crystal structure (Bushnell et al., 1990), respectively. These larger differences among the structures are contributed mainly by the turn, loop, and coil regions. Similar rms differences within the same range have been recently reported between several crystal and NMR structures of interleukin-4 (Smith et al., 1994).

Implications for Biological Electron Transfer. The models for the crystal structures of horse and tuna cytochrome *c* have been used in model building studies to explore potential structural features that lead to the formation and stabilization of the heterologous protein complex involving cytochrome *c* and cytochrome b_5 (Salemme, 1977; Wendoloski et al., 1987), one of the most studied interprotein electron transfer complexes [e.g., Ng et al. (1977), Mauk et al. (1982, 1986), McLendon and Miller (1985), Rodgers et al. (1988), Rodgers and Sligar (1990), Wuttke et al. (1992) and Willie et al. (1993)]. The lysines thought to be central in the formation of some cytochrome *c* complexes, evident in the horse and tuna structures, are preserved in the model for the solution structure of ferricytochrome *c*. Furthermore, long-lived structural waters have been detected in solution for the oxidized and reduced states of cytochrome *c* and are in roughly analogous positions as the waters seen in the oxidized and reduced tuna crystal structures. Specifically, the so-called catalytic water molecule, implicated in electron transfer, is found in roughly analogous positions in the models for the crystal structure of tuna ferrocytochrome *c* (Takano & Dickerson, 1981b) and the solution structure of horse ferrocytochrome *c* (Qi et al., 1994b). This water molecule is found closer to the iron in the model for the oxidized tuna protein. In contrast, the only long-lived water found at this rough location in the model for the solution structure of oxidized horse cytochrome *c* is found to be closer to the surface of the protein and is farther from the heme iron. This is an unexpected result but must be qualified by two comments. First, refinement of the model with a seventh water molecule with the constraints of Wat-1 in the reduced protein results in convergence. This suggests that the model can accommodate a seventh water molecule. Second, the fact that NOEs are not seen to a water molecule does not eliminate the possibility that a water molecule is present but does require that the residence time of the water be short enough to reduce the intensity of the NOEs to below the detection limit. Further experiments and computations are being carried out to test the possibility of additional water molecule(s) in the heme crevice which have short residence times.

In the reduced protein, there is an interesting bisection of the solvent-accessible surface area of the heme edge by the side chain of Ile-81 at the proposed interaction surface. This is absent in the oxidized protein where the side chain of Ile-81 is restricted to one side of the heme. It is well-known that reduced and oxidized cytochromes *c* show different affinities for cytochrome *c* oxidase and that significant structural rearrangements are occurring at the interface upon electron transfer [see, for example, Michel et al. (1989a,b) and Kornblatt and Luu (1986)]. It is interesting to note that this rearrangement is driven more by a change in the main chain than restricted to a reorganization of the side chain of Ile-81. This surface feature may represent one component of a redox-dependent molecular recognition switch and could represent a more simple molecular recognition device than the "push-button trigger" mechanism proposed by Berghuis and Brayer (1992) and would be linked, by arguments outlined above, to the energetics of the redox process itself. Indeed, a microscopic analysis indicates the presence of a direct thermodynamic linkage between the structure change associated with this molecular recognition switch and the setting of the redox potential of the heme by the protein.

Conclusions. A high-resolution model for the solution structure of horse heart ferricytochrome *c* has been determined by ^{1}H 2D and 3D nuclear magnetic resonance spectroscopy combined with hybrid distance geometry−simulated annealing calculations. The overall protein fold is highly homologous to previously determined structures of *c*-type cytochromes. The protein displays several previously undocumented features that differ from those seen in crystal structures of homologous *c*-type cytochromes. These include differences in hydrogen bonding, interhelical contacts, and a number of surface features. Many aspects of the solution structure conform to their counterparts in the crystal structures of homologous *c*-type cytochromes including details of heme ligation, placement of water molecules in the interior of the protein, and many tertiary hydrogen-bonding contacts. All of these have important implications for the electron transfer process, the setting of the heme redox potential, and the recognition of electron transfer partners by the protein. In addition, the model presented here and its counterpart for the reduced protein will provide a detailed template for the interpretation of the internal dynamics of the protein and the evaluation of a variety of redox-linked molecular properties by computational methods such as solvent reorganization energy calculations (Muegge et al., in preparation).

ACKNOWLEDGMENT

We are grateful to Dr. Yiqing Feng for helpful discussion.

SUPPORTING INFORMATION AVAILABLE

Three tables containing an analysis of hydrogen bonding and one table summarizing the updated refinement statistics of the structural model for ferrocytochrome *c* (8 pages). Ordering information is given on any current masthead page.

REFERENCES

Baker, E. N., & Hubbard, R. E. (1984) *Prog. Biophys. Mol. Biol. 44*, 97−179.

Beckman, R. A., Litwin, S., & Wand, A. J. (1993) *J. Biomol. NMR 3*, 675−700.

Berghuis, A. M., & Brayer, G. D. (1992) *J. Mol. Biol. 223*, 959−976.

Bernstein, F. C., Koetzle, T. F., Williams, G. J. B., Meyer, E. F., Bruce, M. D., Rodgers, J. R., Kennard, O., Shimanouchi, T., & Tasmui, M. (1977) *J. Mol. Biol. 112*, 535−542.

Brünger, A. T. (1992) *X-PLOR version 3.1. A system for crystallography and NMR*, Yale University, New Haven, CT.

Bushnell, G. W., Louie, G. V., & Brayer, G. D. (1990) *J. Mol. Biol. 214*, 585−595.

Clore, G. M., & Gronenborn, A. M. (1993) *J. Mol. Biol. 231*, 82−102.

Crippen, G. M. (1978) *J. Comput. Phys. 26*, 449−452.

Dellwo, M. J., & Wand, A. J. (1993) *J. Am. Chem. Soc. 115*, 1886−1893.

Farid, R., Moser, C. C., & Dutton, P. L. (1993) *Cur. Opin. Struct. Biol. 3*, 225−233.

Feng, Y., & Englander, S. W. (1990) *Biochemistry 29*, 3505−3509.

Feng, Y., Roder, H., Englander, S. W., Wand, A. J., & Di Stefano, D. L. (1989) *Biochemistry 28*, 195−203.

Feng, Y., Roder, H., & Englander, S. W. (1990) *Biochemistry 29*, 3494−3504.

Fiori, W. R., Miick, S. M., & Millhauser, G. L. (1993) *Biochemistry 32*, 11957−11962.

Gochin, M., & Roder, H. (1995) *Protein Sci. 4*, 296−305.

Havel, T. F. (1991) *Prog. Biophys. Mol. Biol. 56*, 43−78.

Karplus, M. (1959) *J. Chem. Phys. 30*, 11−15.

Kassner, R. J. (1972) *Proc. Natl. Acad. Sci. U.S.A. 69*, 2263−2267.

Kornblatt, J. A., & Luu, H. A. (1986) *Eur. J. Biochem. 159*, 407−413.

Korszun, Z. R., Bunker, G., Khalid, S., Scheidt, W. R., Cusanovich, M. A., & Meyer, T. E. (1989) *Biochemistry 28*, 1513−1517.

Kraulis, P. J. (1991) *J. Appl. Crystallogr. 24*, 946−950

Macura, S., & Ernst, R. R. (1980) *Mol. Phys. 41*, 95−117.

Mauk, M. R., Reid, L. S., & Mauk, A. G. (1982) *Biochemistry 21*, 1843−1846.

Mauk, M. R., Mauk, A. G., Weber, P. C., & Matthew, J. B. (1986) *Biochemistry 25*, 7085−7091.

McLendon, G., & Miller, J. R. (1985) *J. Am. Chem. Soc. 107*, 7811−7816.

Michel, B., Mauk, A. G., & Bosshard, H. R. (1989a) *FEBS Lett. 243*, 149−152.

Michel, B., Proudfoot, A. E. I., Wallace, C. J. A., & Bosshard, H. R. (1989b) *Biochemistry 28*, 456−462.

Nerdal, W., Hare, D. R., & Reid, B. R. (1988) *J. Mol. Biol. 201*, 717−739.

Neuhaus, D., Wagner, G., Vasák, M., Kägi, H. R., & Wüthrich, K. (1985) *Eur. J. Biochem. 151*, 257−273.

Ng, S., Smith, M. B., Smith, H. T., & Millet, F. (1977) *Biochemistry 16*, 4975−4978.

Nilges, M., Clore, G. M., & Gronenborn, A. M. (1988) *FEBS Lett. 229*, 317−324.

Onuchic, J. N., Winkler, J. R., & Gray, H. B. (1992) *Annu. Rev. Biophys. Biomol. Struct. 21*, 349−377.

Pardi, A., Billeter, M., & Wüthrich, K. (1984) *J. Mol. Biol. 180*, 741−751.

Pavone, V., Benedetti, E., Diblasio, B., Pedone, C., Santini, A., Bavoso, A., Toniolo, C., Crisma, M., & Sartore, L. (1990) *J. Biomol. Struct. Dyn. 7*, 1321−1331.

Pelletier, H., & Kraut, J. (1992) *Science 258*, 1748−1755.

Qi, P. X., Di Stefano, D. L., & Wand, A. J. (1994a) *Biochemistry 33*, 6408−6417.

Qi, P. X., Fuentes, E. J., Urbauer, J. L., Leopold, M. F., & Wand, A. J. (1994b) *Nat. Struct. Biol. 1*, 378−382.

Rance, M., Sørensen, O. W., Bodenhausen, G., Wagner, G., Ernst, R. R., & Wüthrich, K. (1983) *Biochem. Biophys. Res. Commun. 117*, 479−485.

Roder, H., Elöve, G. A., & Englander, S. W. (1988) *Nature 335*, 700−704.

Rodgers, K. K., & Sligar, S. G. (1991) *J. Mol. Biol. 221*, 1453−1460.

Rodgers, K. K., Pochapsky, T. C., & Sligar, S. G. (1988) *Science 240*, 1657−1659.

Salemme, R. (1977) *J. Mol. Biol. 102*, 563−568.

Stikle, D. F., Presta, L. G., Dill, K. A., & Rose, G. D. (1992) *J. Mol. Biol. 220*, 1143−1159.

Takano, T., & Dickerson, R. E. (1981a) *J. Mol. Biol. 153*, 79−94.

Takano, T., & Dickerson, R. E. (1981b) *J. Mol. Biol. 153*, 95−114.

Vuister, G. W., Boelens, R., & Kaptein, R. (1988) *J. Magn. Reson. 80*, 176−185.

Wand, A. J., & Englander, S. W. (1985) *Biochemistry 24*, 5290−5294.

Weber, P. L., Morrision, R., & Hare, D. R. (1988) *J. Mol. Biol. 204*, 483−487.

Wendoloski, J. J., Matthew, J. B., Weber, P. C., & Salemme, F. R. (1987) *Science 238*, 794−797.

Williams, G. C. N., Moore, G. R., & Williams, R. J. P. (1985) *J. Mol. Biol. 183*, 447−460.

Willie, A., McLean, M., Liu, R.-Q., Hilegn-Willis, S., Saunders, A. J., Pielak, G. J., Sligar, S. G., Durham, B., & Millet, F. (1993) *Biochemistry 32*, 7519−7525.

Wu, L. C., Laub, P. B., Elove, G. A., Carey, J., & Roder, H. (1993) *Biochemistry 32*, 10271−10276.

Wuttke, D. S., Bjerrum, M. J., Winkler, J. R., & Gray, H. B. (1992) *Science 256*, 1007−1009.

BI961042W